Toxicology Letters 295 (2018) 357–368

Contents lists available at ScienceDirect

Toxicology Letters

journal homepage: www.elsevier.com/locate/toxlet

Heme Oxygenase-1 protects astroglia against manganese-induced oxidative injury by regulating mitochondrial quality control

Roxana Mayra Gorojod[a,3], Agustina Alaimo[a,1,3], Soledad Porte Alcon[a], Jimena Hebe Martinez[b], María Eugenia Cortina[a,2], Elba Susana Vazquez[c], Mónica Lidia Kotler[a,*]

[a] CONICET- Universidad de Buenos Aires, Instituto de Química Biológica Ciencias Exactas y Naturales (IQUIBICEN), Facultad de Ciencias Exactas y Naturales, Departamento de Química Biológica, Laboratorio de Disfunción Celular en Enfermedades Neurodegenerativas y Nanomedicina. Buenos Aires, Argentina

[b] CONICET- Universidad de Buenos Aires, Instituto de Química Biológica Ciencias Exactas y Naturales (IQUIBICEN), Facultad de Ciencias Exactas y Naturales, Departamento de Química Biológica (CM1). Laboratorio Interdisciplinario de Dinámica Celular y Nanoherramientas. Buenos Aires, Argentina

[c] CONICET- Universidad de Buenos Aires, Instituto de Química Biológica Ciencias Exactas y Naturales (IQUIBICEN), Facultad de Ciencias Exactas y Naturales, Departamento de Química Biológica (CM1), Laboratorio de Inflamación y Cáncer. Buenos Aires, Argentina

ARTICLE INFO

Keywords:
Heme Oxygenase-1
Mitochondrial quality control
Oxidative stress
Astroglia
Manganese
Manganism

ABSTRACT

Heme Oxygenase-1 (HO-1), a stress- responsive enzyme which catalyzes heme degradation into iron, carbon monoxide, and biliverdin, exerts a neuroprotective role involving many different signaling pathways. In Parkinson disease patients, elevated HO-1 expression levels in astrocytes are involved in antioxidant defense. In the present work, employing an *in vitro* model of Mn^{2+}-induced Parkinsonism in astroglial C6 cells, we investigated the role of HO-1 in both apoptosis and mitochondrial quality control (MQC). HO-1 exerted a protective effect against Mn^{2+} injury. In fact, HO-1 decreased both intracellular and mitochondrial reactive oxygen species as well as the appearance of apoptotic features. Considering that Mn^{2+} induces mitochondrial damage and a defective MQC has been implicated in neurodegenerative diseases, we hypothesized that HO-1 could mediate cytoprotection by regulating the MQC processes. Results obtained provide the first evidence that the beneficial effects of HO-1 in astroglial cells are mediated by the maintenance of both mitochondrial fusion/fission and biogenesis/mitophagy balances. Altogether, our data demonstrate a pro-survival function for HO-1 in Mn^{2+}-induced apoptosis that involves the preservation of a proper MQC. These findings point to HO-1 as a new therapeutic target linked to mitochondrial pathophysiology in Manganism and probably Parkinson´s disease.

1. Introduction

Heme Oxygenase-1 (HO-1) is a stress-responsive enzyme that catalyzes the rate-limiting step of heme degradation into biliverdin/bilirubin, free iron and CO (Tenhunen et al., 1968; Ryter and Choi, 2002). Its expression is induced by a wide array of pro-oxidant and inflammatory stimuli in order to generate adaptive responses against stress in many different cell types (for references, see Gozzelino et al., 2010). The beneficial effects of HO-1 are not merely due to heme degradation but also to its end products, particularly CO and biliverdin/bilirubin, which exert potent anti-oxidant, anti-inflammatory and anti-apoptotic effects (Agarwal and Bolisetty, 2013). Nevertheless, it should be noted that elevated brain HO-1 levels constitute an anatomopathological feature of neurodegenerative disorders such as Parkinson and Alzheimer diseases. Whether HO-1 induction in neurodegeneration leads to redox homeostasis restoration or to pathological free iron deposition and bioenergetic failure, still remains elusive (Cuadrado and Rojo, 2008; Schipper, 2011; Hettiarachchi et al., 2017).

Manganism is a neurodegenerative disorder caused by chronic exposure to manganese (Mn) which clinically resembles Parkinson's

* Corresponding autor at: Avda, Ciudad Universitaria, Intendente Güiraldes 2160, Buenos Aires, C1428EGA, Argentina.
E-mail addresses: rgorojod@qb.fcen.uba.ar (R.M. Gorojod), aalaimo@qb.fcen.uba.ar (A. Alaimo), sportealcon@qb.fcen.uba.ar (S. Porte Alcon), jhebemartinez@gmail.com (J.H. Martinez), archaeopteryxvivo@hotmail.com (M.E. Cortina), elba@qb.fcen.uba.ar (E.S. Vazquez), moniquekotler@gmail.com, kotler@qb.fcen.uba.ar (M.L. Kotler).

[1] Present addresses: CONICET- Universidad de Buenos Aires. Instituto de Química Biológica Ciencias Exactas y Naturales (IQUIBICEN). Facultad de Ciencias Exactas y Naturales, Departamento de Química Biológica (CM1). Laboratorio Interdisciplinario de Dinámica Celular y Nanoherramientas. Buenos Aires, Argentina.

[2] CONICET- Universidad Nacional de San Martín. Instituto de Investigaciones Biotecnológicas Dr. Rodolfo A. Ugalde, Instituto Tecnológico de Chascomús (IIB-INTECH). San Martín, Buenos Aires, Argentina.

[3] These authors contributed equally to this work.

https://doi.org/10.1016/j.toxlet.2018.07.045
Received 18 June 2018; Received in revised form 16 July 2018; Accepted 21 July 2018
Available online 21 July 2018

disease. Mn overexposure often occurs under certain occupational and environmental settings causing its accumulation in the central nervous system (CNS), predominantly in the basal ganglia (Roth, 2009). Mn preferentially concentrates in astrocytes given the expression of high-capacity transporters in these cells. As a consequence, astrocytes present intracellular Mn levels 50–60 fold higher than neurons (Aschner et al., 1992). Thus, astrocytes have been proposed as initial targets of Mn neurotoxicity which may induce and/or exacerbate neuronal dysfunction (Milatovic et al., 2007). Mn cytotoxicity involves oxidative stress, mitochondrial damage, and apoptotic cell death (Alaimo et al., 2011, 2014; Gunter et al., 2006; Milatovic et al., 2007; Roth, 2009).

Mitochondria are crucial for many essential cellular processes, including ATP synthesis, energy metabolism, redox signaling, and cell death. Its proper functioning is maintained by the mitochondrial quality control (MQC) machinery, an integrated network of pathways involving mitochondrial dynamics, biogenesis and mitophagy (Palikaras et al., 2015). Impairments in these quality control systems may produce defective mitochondria accumulation, as well as failed mitochondrial transport and distribution, leading to neuronal degeneration and onset of several neurodegenerative diseases (Dupuis, 2014; Suliman and Piantadosi, 2016).

Previous work from our group showed increased mitochondrial fission and mitophagy in Mn^{2+}-exposed astroglial cells, suggesting that an imbalance in the MQC mechanisms is involved in cellular damage (Alaimo et al., 2014; Gorojod et al., 2017). Based on this evidence and the recent research describing a protective role for HO-1 by regulating the MQC balance (Hull et al., 2016), we aimed to establish the possible induction of HO-1 in astroglial C6 cells challenged with Mn^{2+} with special focus on mitochondrial integrity and MQC regulation. Our results show for the first time that HO-1 is relevant for astroglial cell survival after Mn^{2+} exposure by counteracting ROS production and inhibiting apoptosis. We also demonstrate that HO-1 confers broad protective effects in MQC. These results would be relevant for the design of new therapeutic strategies aimed to improve mitochondrial integrity and upregulate cellular defenses both in Manganism and other neurodegenerative diseases.

2. Material and methods

2.1. Reagents

Dulbecco's Modified Eagle's Medium (DMEM), trypsin, manganese chloride, hemin from bovine, 3-(4,5-dimethyl-thiazol-2-yl)-2,5-diphenyl-tetrazolium bromide (MTT), Hoechst 33258 fluorochrome, 2′,7′-dichlorodihydrofluorescein diacetate (DCDHF-DA) and ECL detection reagents (luminol and p-coumaric acid) were purchased from Sigma-Aldrich Co. (St. Louis, MO, USA). Sn(IV) Protoporphyrin IX dichloride (SnPP) was from Frontier Scientific Europe Ltd. (Lancashire, UK). Fetal bovine serum (FBS) was obtained from Natocor (Córdoba, Argentina). Streptomycin, penicillin and amphotericin B were from Richet (Buenos Aires, Argentina). N-(2-hydroxyethyl) piperazine-N´-(2-ethane-sulfonic acid) (HEPES) was from ICN Biomedicals (Irvine, CA, USA). SB203580, SP600125, PD98059 and LY294002 inhibitors were from Calbiochem (La Jolla, CA, USA). MitoTracker Red CMXRos and MitoSOX Red were from Molecular Probes (Eugene, OR, USA).

The following antibodies were employed: anti-HO-1 (StressGen Bioreagents Corp, Victoria, BC, Canada); anti-p-JNK (G7) sc-6254, anti-p-ERK (E-4) sc-7383, anti-p-p38 (Thr 180/Tyr 182) sc-17852-R, anti-JNK1 (G-13) sc-46006, anti-ERK2 (C-14) sc-154, anti-p38 (N-20) sc-728, anti-NRF-1 (H-300) sc-33771, anti-β-Actin (C4) sc-47778, anti-MAP LC3β sc-16755, anti-TOM-20 (FL-145) sc-11415, anti-rabbit IgG-HRP sc-2030, anti-mouse IgG-HRP sc-2031, anti-goat IgG-HRP sc-2020 (Santa Cruz Biotechnology); anti-Akt #9272, anti-phospho-Akt (Ser473) #9271 (Cell Signaling Technology, Danvers, MA, USA); Alexa fluor 488 donkey anti-goat (A-11055), Alexa Fluor 555 goat anti-rabbit IgG (H + L) (Molecular Probes); anti-PGC1-α (101707) (Cayman Chemical Company).

2.2. Cell culture

Rat C6 cells (ATCC CCL-107) were maintained in DMEM supplemented with 10% heat-inactivated FBS, 2.0 mM glutamine, 100 units/ml penicillin, 100 µg/ml streptomycin and 2.5 µg/ml amphotericin B. Cells were cultured at 37 °C in a humidified atmosphere of 5% CO_2-95% air, and the medium was renewed three times a week. For all experiments, C6 cells were removed with 0.25% trypsin-EDTA diluted with DMEM 10% FBS and re-plated into multi-well plates. After 24 h, 70–80% confluent cultures were exposed to 750 µM $MnCl_2$ (Mn^{2+}) in serum free (SF) media.

All experiments containing SnPP or hemin were conducted in the dark with a dim light to minimize inactivation of these compounds. Cell culture plates or petri dishes were kept in the dark.

2.3. Plasmids and transfections

The human pcDNA3 HO-1 expression vector was kindly provided by Dr. M. Mayhofer (Clinical Institute for Medical and Chemical Laboratory Diagnostics, University of Vienna, Vienna, Austria).

For transfections, C6 cells were seeded and allowed to grow for 24 h until 50–60% confluence. Transfection complexes were prepared in SF media in a ratio PEI:DNA 3.75:1. Mixtures were vortexed, incubated 10 min at RT and then drop-wise added to the cells in S serum supplemented media. After 5 h, media was renewed. Mn^{2+} exposure was conducted at 24 h post-transfection.

2.4. Assessment of cell viability by MTT assay

The conversion of MTT to formazan by mitochondrial dehydrogenases was used as an index of cell viability according to the protocol previously described (Alaimo et al., 2011). After exposure, cells grown on 96-well plates were washed with PBS and incubated with MTT (0.125 mg/ml) in culture media for 90 min at 37 °C. Then, media was removed and formazan was solubilized in 200 µl of DMSO. Absorbance was measured at 570 nm with background subtraction at 655 nm in a BIO-RAD Model 680 Benchmark microplate reader (BIO-RAD laboratories, Hercules, CA, USA). The MTT reduction activity was expressed as a percentage of control cells.

2.5. Western blotting

Western blots were performed according to the protocol described (Alaimo et al., 2011; Gorojod et al., 2015). Briefly, cells were suspended in lysis buffer (50 mM HEPES/ 0.1% Triton X-100 pH 7.0, 0.5 mM PMSF, 10 µg/ml aprotinin and 10 µg/ml benzamidine), incubated for 30 min at 4 °C and sonicated. After centrifugation (10,000xg, 20 min, 4 °C), protein concentration was determined using the Bradford assay. Equal amounts of protein (60–80 µg) from each treatment were separated by 10–12% SDS-polyacrylamide gel electrophoresis (SDS-PAGE) and blotted onto nitrocellulose membranes (Hybond ECL, GE Healthcare, NJ, USA). Transference efficiency was verified by staining the membrane with Ponceau Red. Non-specific binding sites were blocked by 5% non-fat dried milk in TBS (150 mM NaCl in 50 mM Tris-HCl buffer pH 8) containing 0.1% SDS, for 90 min and then incubated with specific antibodies overnight (ON) at 4 °C. The primary antibody reaction was followed by incubation for 1 h with horseradish peroxidase-conjugated secondary antibodies. All antibodies were diluted in TBST (150 mM NaCl, 0.05% Tween 20, in 10 mM Tris-HCl buffer pH 8) with 3% non-fat dried milk. Immunoreactive bands were detected employing enhanced chemiluminescence western blotting detection reagents (ECL). Images were captured with the luminescent LAS 1000 plus Image Analyser employing LAS 1000 pro software (Fuji, Tokyo, Japan). Quantitative changes in protein levels were evaluated employing

ImageJ software (NIH). The molecular weight of proteins was estimated by electrophoresis of protein markers (Fermentas Life Sciences, CA, USA).

2.6. Detection of apoptotic cells by fluorescence microscopy

The analysis of nuclear morphology was assessed as described (Alaimo et al., 2011). Cells were sub-cultured on glass coverslips in 12-well plates at a density of 6×10^4 cells/well. After treatments, cells were washed with PBS and fixed with 4% paraformaldehyde/4% sucrose (4% PFA) for 20 min at room temperature (RT). Then, cells were washed twice with PBS and stained with Hoechst 33258 (1 µg/ml, 10 min). Finally, coverslips were washed and mounted in PBS-glycerol (1:1, v/v). Images were analyzed employing an Olympus IX71 microscope equipped with objective lens 100X/1.65 oil (λ_{ex}: 350/50 nm; λ_{em}: 460/50 nm) (Olympus Corporation, Tokyo, Japan). Images were captured with a Hamamatsu Photonics ORCA-ER camera (Hamamatsu Photonics K.K., Systems Division, Hamamatsu, Japan). Digital pictures were analyzed and assembled using Adobe Photoshop 7.0 software. Cells with uniformly stained nuclei were scored as viable (normal), whereas those with condensed or fragmented nuclei were considered as apoptotic cells.

2.7. Cellular and mitochondrial reactive oxygen species (ROS) detection

2.7.1. Total ROS levels

Intracellular ROS production was measured by the oxidation of DCDHF-DA to the highly fluorescent compound 2′,7′-dichlorofluorescein (DCF). After treatments, cells grown on coverslips were incubated with DCDHF-DA 10 µM for 30 min at 37 °C in the dark. Samples were observed using a Nikon Eclipse E600 microscope (Nikon Instech Co., Ltd., Karagawa, Japan) employing FITC filters (λ_{ex}: 450–490 nm; λ_{em}: 515 nm). Images were captured with a Nikon CoolPix5000 digital camera and the average DCF fluorescence intensity was calculated employing ImageJ software.

2.7.2. Mitochondrial ROS production

MitoSOX Red, a cationic derivative of dihydroethidium (DHE), is a dye used to determine mitochondrial-derived superoxide anion ($O_2^{\bullet -}$) generation. It reacts with $O_2^{\bullet -}$ faster than DHE and is rapidly targeted to the mitochondria, where it is oxidized by $O_2^{\bullet -}$ to form 2-hydroxymitoethidium, which excites and emits at 510 and 580 nm, respectively. MitoSOX Red can also undergo unspecific reactions with other oxidants to form mito-ethidium, which overlaps the 2-hydroxymitoethidium fluorescence peak (510 nm). Thus, it has been proposed another specific excitation peak at 400 nm for 2-hydroxymitoethidium (Robinson et al., 2008). Therefore, two different excitation wavelengths are used to distinguish the $O_2^{\bullet -}$ and other oxidative products. After treatments, cells were loaded with MitoSox Red 5 µM for 10 min at 37 °C in the dark. Fluorescence intensity of the cell lysates was measured in a FLUOstar OPTIMA fluorometer (BMG LABTECH, Ortenberg, Germany) (λ_{ex}: 510 nm or 400 nm; λ_{em}: 590 nm). Values were normalized to the total amount of proteins determined by Bradford assay.

2.8. Mitochondrial integrity and morphometric analysis

After Mn^{2+} exposure, cells grown on coverslips were washed twice with PBS and incubated with the cell-permeant mitochondria-specific fluorescent probe MitoTracker Red CMXRos (75 nM in SF, 30 min, 37 °C). Afterwards, cells were washed twice with PBS and fixed with 4% PFA (20 min at RT). Finally, cells were washed with PBS and mounted on glass slides. Samples were examined under a fluorescence microscope Olympus IX71 equipped with objective lens 60X/1.43 oil (λ_{ex}: 543/20 nm; λ_{em}: 593/40 nm). Images were captured with a Hamamatsu Photonics ORCA-ER camera. Digital images were optimized for contrast and brightness using Adobe Photoshop 7.0 Software.

Mitochondrial morphology was classified as tubular (normal), intermediate (mixed) or fragmented (small, rounded and/or swollen) mitochondria according to Alaimo et al. (2011, 2014). Cells without probe retention were classified as "loss of mitochondrial membrane potential (Δφm)". A total of 200 cells were scored for each sample.

Morphometric parameters were determined by using the Mito-Morphology Macro of ImageJ software previously described (Dagda et al., 2009). MitoTracker Red CMXRos images were thresholded to optimally resolve individual mitochondria. The area/perimeter ratio and inverse roundness were calculated and employed as indexes of mitochondrial interconnectivity and mitochondrial elongation, respectively.

2.9. Immunocytochemistry

2.9.1. Mitophagy

Double-immunocytochemistry was assessed as described (Gorojod et al., 2015). Fixed samples were permeabilized with Triton X-100 0.25% in PBS (10 min, RT), washed 3 times with PBS (5 min) and blocked with 1% BSA in PBST (Tween 20 0.1% in PBS) ON at 4 °C. Coverslips were incubated with a solution of anti-MAP LC3β and anti-TOM-20 (1:100 and 1:500, respectively) for 1 h at RT, washed 3 times with PBS and incubated with a solution of Alexa 488 anti-goat IgG (1:1000; 1 h, RT in the dark). After 3 washes with PBS, samples were incubated with Alexa 555 anti-rabbit IgG (1:1000; 1 h, RT in the dark). Finally, coverslips were washed three times with PBS and mounted with a solution of PBS- glycerol (1:1, v/v). Samples were analyzed under a FV300 confocal fluorescence microscope (Olympus Optical Co.) equipped with the image acquisition software Fluoview 5.0 (Olympus Optical Co.). An Olympus 60x oil-immersion Plan Apo objective (numerical aperture: 1.4) was employed. Sequential scanning of slices with Argon (λ: 488 nm) and Helium-Neon (λ: 543 nm) lasers was performed to reduce bleed-through of the fluorescence signal. Manders' overlap coefficient (R) was calculated employing the intensity correlation analysis plug-in for ImageJ software (U. S. National Institutes of Health, Bethesda, MD, USA) with subtraction of the mean value plus 3x the standard deviation of the background.

2.9.2. Biogenesis

Immunocytochemistry was assessed as described (Alaimo et al., 2013). Fixed samples were permeabilized with 0.25% Triton X-100 in PBST (0.1% Tween 20 in PBS pH 7.4) for 10 min at RT and washed three times with PBS (5 min). Non-specific binding sites were blocked with 1% BSA in PBST for 30 min at RT. Coverslips were incubated with anti-PGC-1α or NRF-1 antibodies (ON, 4 °C), washed three times with PBS and then incubated with an Alexa 555 anti-rabbit IgG antibody (1 h, RT) in the dark. Finally, nuclei were counterstained employing Hoechst 33258 fluorescent probe. After washing with PBS, coverslips were mounted with PBS-glycerol (1:1, v/v). Samples were examined under a fluorescence microscope Olympus IX71 (Alexa 555, λ_{ex}: 543/20 nm, λ_{em}: 593/40 nm; Hoechst 33258, λ_{ex}: 350/50 nm; λ_{em}: 460/50 nm). The nuclear compartment was selected and fluorescence intensity was calculated employing ImageJ software.

2.10. Statistical analysis

Experiments were carried out in triplicate unless otherwise stated. Results are expressed as mean ± standard error of the mean (SEM) values. Experimental comparisons between treatments were made by Student's *t*-test or one-way ANOVA, followed by Student-Newman-Keuls *post hoc* test with statistical significance set at $p < 0.05$. All analyses were carried out with GraphPad Prism 5 software (San Diego, CA, USA).

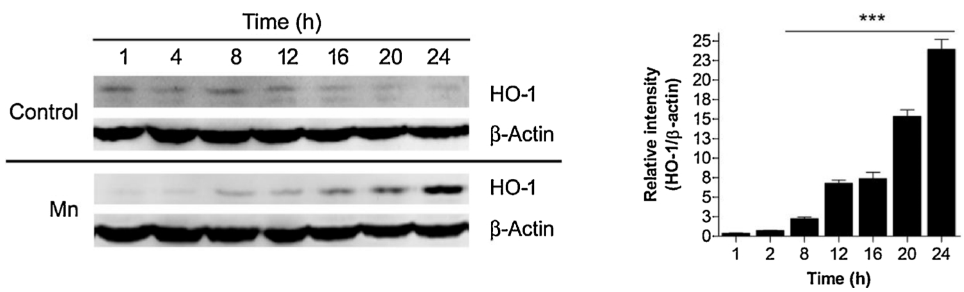

Fig. 1. Mn^{2+} increases HO-1 levels in C6 cells. Cells were exposed to 750 μM Mn^{2+} for 1–24 h. Cell lysates were run on SDS-PAGE and transferred to nitrocellulose membranes. HO-1 expression was analyzed and normalized to β-Actin. ***$p < 0.001$ vs. control.

3. Results

3.1. HO-1 is cytoprotective against Mn^{2+}-induced toxicity

The up-regulation of HO-1 plays a key role in protecting cells against toxicity caused by oxidative insults (Gozzelino et al., 2010). In the present work, C6 cells were exposed to 750 μM Mn^{2+} for 1–24 h and HO-1 expression levels were evaluated by western blot (Fig. 1). Mn^{2+} induced a time-dependent increase in HO-1 levels, ranging from two-fold at 8 h ($p < 0.001$) to 23-fold after 24 h ($p < 0.001$).

HO-1 has been reported as a metabolic double-edged sword with beneficial or detrimental effect on cell physiology (Wagener et al., 2003). To determine the effect of HO-1 induction in Mn^{2+} toxicity we first employed SnPP, a specific competitive pharmacological HO-1 inhibitor (Kappas et al., 1984). SnPP (10–50 μM) enhanced Mn^{2+} cytotoxicity measured by MTT assay (Fig. 2A). Particularly, 50 μM SnPP increased 14 ± 4% ($p < 0.05$) Mn^{2+}-induced cell death after 24 h exposure. Considering that SnPP has previously shown to increase HO-1 expression (Sardana and Kappas, 1987), we next analyzed this effect. As shown in Fig. 2B, SnPP *per se* induced HO-1 expression in a concentration-dependent manner. However, in the presence of Mn^{2+}, SnPP decreased Mn^{2+}-induced HO-1 up-regulation for all the concentrations tested.

As we have mentioned above, Mn^{2+} induces apoptotic cell death in C6 cells (Alaimo et al., 2011). Thus, nuclear staining with Hoechst 33,258 was performed in order to analyze the effect of HO-1 inhibition on apoptosis (Fig. 2C). Control cells exhibiting normal shaped and uniformly stained chromatin were distinguished from apoptotic cells presenting condensed and fragmented nuclei. Treatment with 50 μM SnPP increased the occurrence of apoptosis in Mn^{2+}-exposed cells, in accordance with the reduction in cell viability observed on the MTT assay (Fig. 2A).

Then, we carried out experiments to study the effect of HO-1 induction (Tenhunen et al., 1970). For this purpose, cells were pre-incubated with hemin (10–100 μM), exposed to 750 μM Mn^{2+} for 24 h and cell viability was measured by MTT assay. 80 μM hemin prevented Mn^{2+}-induced cell death (15 ± 6%; $p < 0.01$) and increased HO-1 expression (18-fold; $p < 0.001$) (Figs. 3**A and B**). Moreover, hemin by its own did not exert toxicity for all the concentration range tested, in accordance with data obtained by Morita et al. (2009). In order to add evidence about the protective action of HO-1 upregulation, cells were transfected with a pcDNA3-HO-1 expression plasmid and then exposed to Mn^{2+}. HO-1 overexpression diminished 25 ± 12% Mn^{2+}-induced cell death ($p < 0.01$) supporting the results obtained by hemin treatment (Fig. 3**C and D**). Finally, we explored the effects of 80 μM hemin on the number of apoptotic nuclei. Our results showed that hemin treatment diminished the number of condensed and fragmented nuclei in Mn^{2+}-exposed cells (12 ± 2%; $p < 0.05$) (Fig. 3E).

Data obtained in Figs. 2 and 3 demonstrates that HO-1 plays a relevant role counteracting Mn^{2+}-induced apoptotic cell death in astrocytoma C6 cells. Moreover, both pharmacological and genetic enzyme upregulation were effective to diminish Mn^{2+} toxicity. Thus, we next investigated the signaling pathways involved in Mn^{2+}-induced HO-1 induction.

3.2. ERK, p38 and PI3K/Akt pathways positively modulate HO-1 expression

The mitogen-activated protein kinases (MAPKs) are intermediate targets on the pathway to *Hmox1* gene regulation (Ryter et al., 2006). This protein family is composed by the extracellular signal-regulated kinase (ERK), c-Jun NH2-terminal kinase (JNK), and p38. These kinases play central roles in the signaling pathways involved in cell proliferation, autophagy, differentiation, survival and apoptosis (Wada and Penninger, 2004; Sridharan et al., 2011). As shown in Fig. 4A, Mn^{2+} treatment induced both ERK (p42: 157%, $p < 0.001$) and JNK (p54: 45%, $p < 0.01$; p46: 89%, $p < 0.001$) activation, whereas no significant changes in p38 were detected. On this basis, and considering that MAPKs can positively or negatively regulate HO-1 (Ryter et al., 2002; Zhang et al., 2002), we investigated the effect of MAPKs inhibitors on HO-1 expression (Fig. 4B). Immunoblot analysis revealed that ERK (PD98059, 25 μM) and p38 (SB203580, 10 μM) inhibition partially prevented HO-1 induction (36 ± 7% and 30 ± 3% $p < 0.01$, respectively) while JNK inhibitor (SP600125, 20 μM) did not exert any effect.

The phosphatidylinositol 3-kinase (PI3K)/Akt pathway, which plays a critical role in cell survival after multiple apoptotic insults, has also been associated to *Hmox1* gene transcription under oxidative stress conditions (Martin et al., 2004). By immunoblotting, we demonstrated that Mn^{2+} induced a decrease in pAkt levels (42 ± 4%; $p < 0.01$) (Fig. **4**C). Moreover, pre-incubation with the PI3K inhibitor LY294002 (20 μM) prevented HO-1 induction (19 ± 3%; $p < 0.01$) (Fig. **4**D) and increased Mn^{2+}-induced cell death (18 ± 3%, $p < 0.01$) (Fig. **4**E).

Overall, these results point to ERK, p38 and PI3K/Akt as modulators of HO-1 expression in our model. However, while PI3K/Akt is relevant for cell viability, neither p38 nor ERK pathways have impact on this parameter (data not shown).

3.3. Hemin prevents ROS generation and Mn2+-induced mitochondrial dysfunction

We have demonstrated that oxidative stress plays a critical role in the onset of Mn^{2+}-induced apoptosis in C6 cells (Alaimo et al., 2011). Considering that HO-1 expression is expected to contribute to the maintenance of redox homeostasis, we evaluated the effect of hemin on ROS production. By employing the oxidation-sensitive probe DCDHF-DA, we determined that hemin reduced (20 ± 3%; $p < 0.05$) the intracellular ROS generated by Mn^{2+} (Fig. 5**A**). Moreover, the increase in mitochondrial ROS induced by Mn^{2+} exposure (48 ± 13%, $p < 0.01$ and 55 ± 13% $p < 0.001$, measured at λ_{ex}: 510 nm and 400 nm respectively) was completely prevented by hemin treatment (Fig. 5B). To gain information about mitochondrial integrity, we determined Δφm by MitoTracker Red CMXRos staining (Fig. 5C). Results showed that hemin prevented the occurrence of mitochondria exhibiting Δφm dissipation

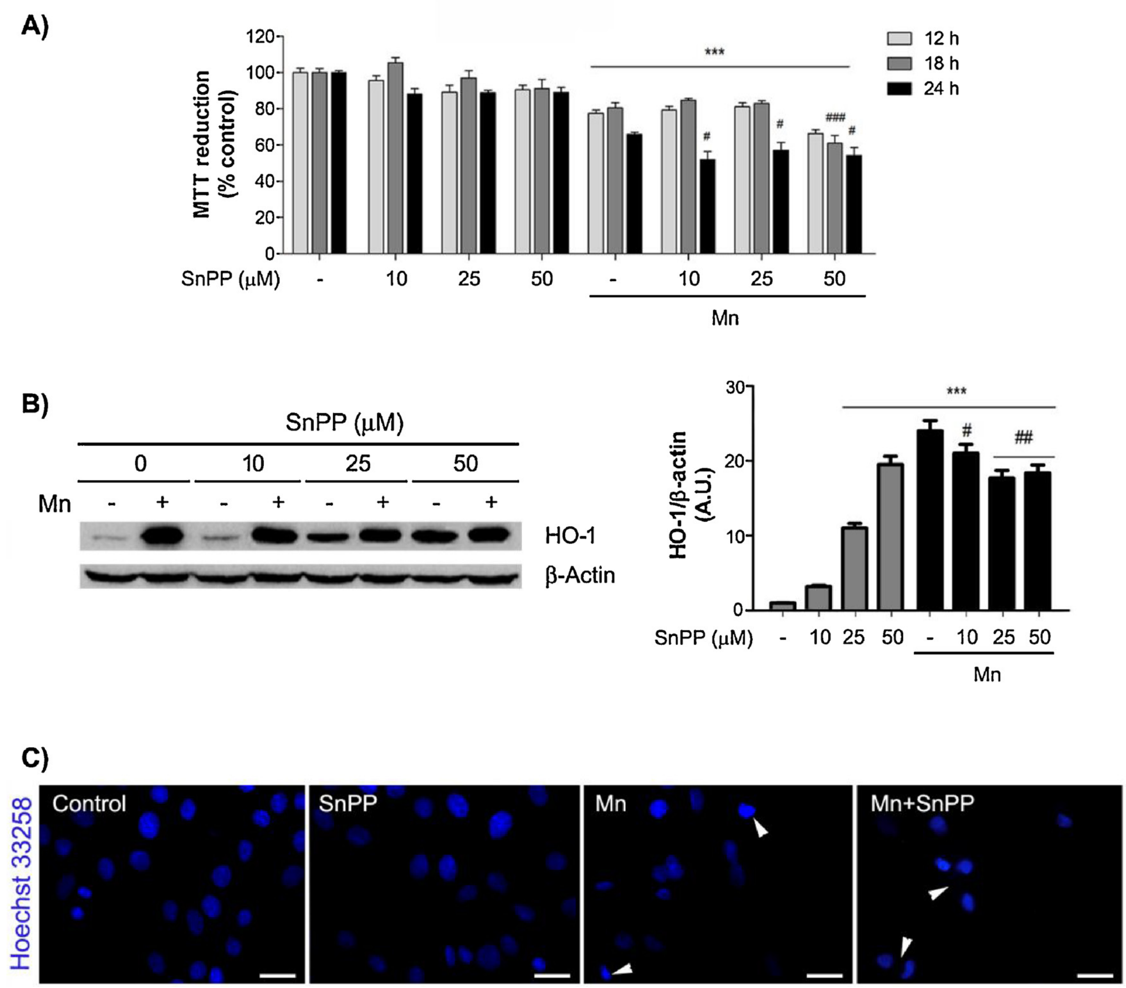

Fig. 2. HO-1 inhibition by SnPP enhances Mn^{2+} injury. Cells were preincubated 1 h with SnPP (10, 25 or 50 μM) and then exposed to Mn^{2+} for 24 h. **A.** Cell viability was measured by MTT assay. **B.** HO-1 expression levels were quantified and normalized to β-Actin. **C.** Normal and apoptotic nuclei (arrowheads) were stained with Hoechst 33,258 (1 μg/ml) and observed by fluorescence microscopy (λ_{em}: 350/50 nm, λ_{ex}: 460/50 nm). Magnification: 100 × . Scale bar: 20 μm. $^{***}p < 0.001$ vs. control; $^{\#}p < 0.05$, $^{\#\#}p < 0.01$, $^{\#\#\#}p < 0.001$ vs. Mn. A.U.: arbitrary units.

(16 ± 2%; $p < 0.001$) in Mn^{2+}-exposed cells. Taken together, these data demonstrate that HO-1 decreases ROS generation and mitochondrial damage induced by Mn^{2+}. Therefore, our next challenge was to determine the underlying mechanisms leading to HO-1 mediated-mitochondrial protection.

3.4. HO-1 plays a role in the maintenance of MQC

3.4.1. Mitochondrial dynamics

The dynamic nature of the mitochondrial network allows its reorganization via fusion and fission processes. Thereby, dysfunctional organelles can be repaired through the fusion with healthy mitochondria, while those severely damaged are segregated by fission and cleared through a specific autophagy mechanism termed mitophagy (Westermann, 2010). We have previously found that Mn^{2+} induces an imbalance in the fusion/fission equilibrium in C6 cells, leading to the mitochondrial network fragmentation (Alaimo et al., 2011, 2014). Considering previous work demonstrating a cytoprotective role for HO-1 in heart by maintaining the MQC (Hull et al., 2016), we first evaluated the effect of hemin on mitochondrial dynamics. Our results demonstrated that pre-incubation with 80 μM hemin decreased 24 ± 8% ($p < 0.05$) the number of cells presenting fragmented mitochondria when compared to Mn^{2+} exposure alone (Fig. 6A). We next employed the NIH ImageJ Mito-Morphology Macro that traces individual mitochondria in an unbiased manner to compute several morphological parameters. Mn^{2+} exposure reduced mitochondrial interconnectivity (15 ± 4%, $p < 0.05$), elongation (60 ± 9%, $p < 0.001$) and mass (53 ± 8%, $p < 0.01$), all of which were prevented by hemin (Fig. 6B).

3.4.2. Mitophagy

Previous findings from our group have demonstrated the occurrence of mitophagy in Mn^{2+}-exposed C6 cells (Gorojod et al., 2015). To evaluate the implication of HO-1 on this MQC program, we determined the degree of co-localization between autophagosomes (LC3) and mitochondria (TOM-20) (Fig. 7A). We found that the Manders´ overlap coefficient (R) was diminished in Mn^{2+}-exposed cells treated with hemin (Mn^{2+}: 0.47 ± 0.05; hemin + Mn^{2+}: 0.34 ± 0.02, $p < 0.01$), indicating a decrease in the number of mitochondrion being eliminated by mitophagy (Fig. 7B). This result suggests the presence of healthier mitochondria in hemin-treated cells.

3.4.3. Biogenesis

Mitochondrial biogenesis is mediated by numerous transcription factors in response to both intracellular signals and environmental stimuli. The master regulator of mitochondrial energy metabolism is the peroxisome proliferator-activated receptor gamma co-activator 1-alpha (PGC-1α), a member of the peroxisome proliferator activated receptor family of transcription co-activators. This protein orchestrates the

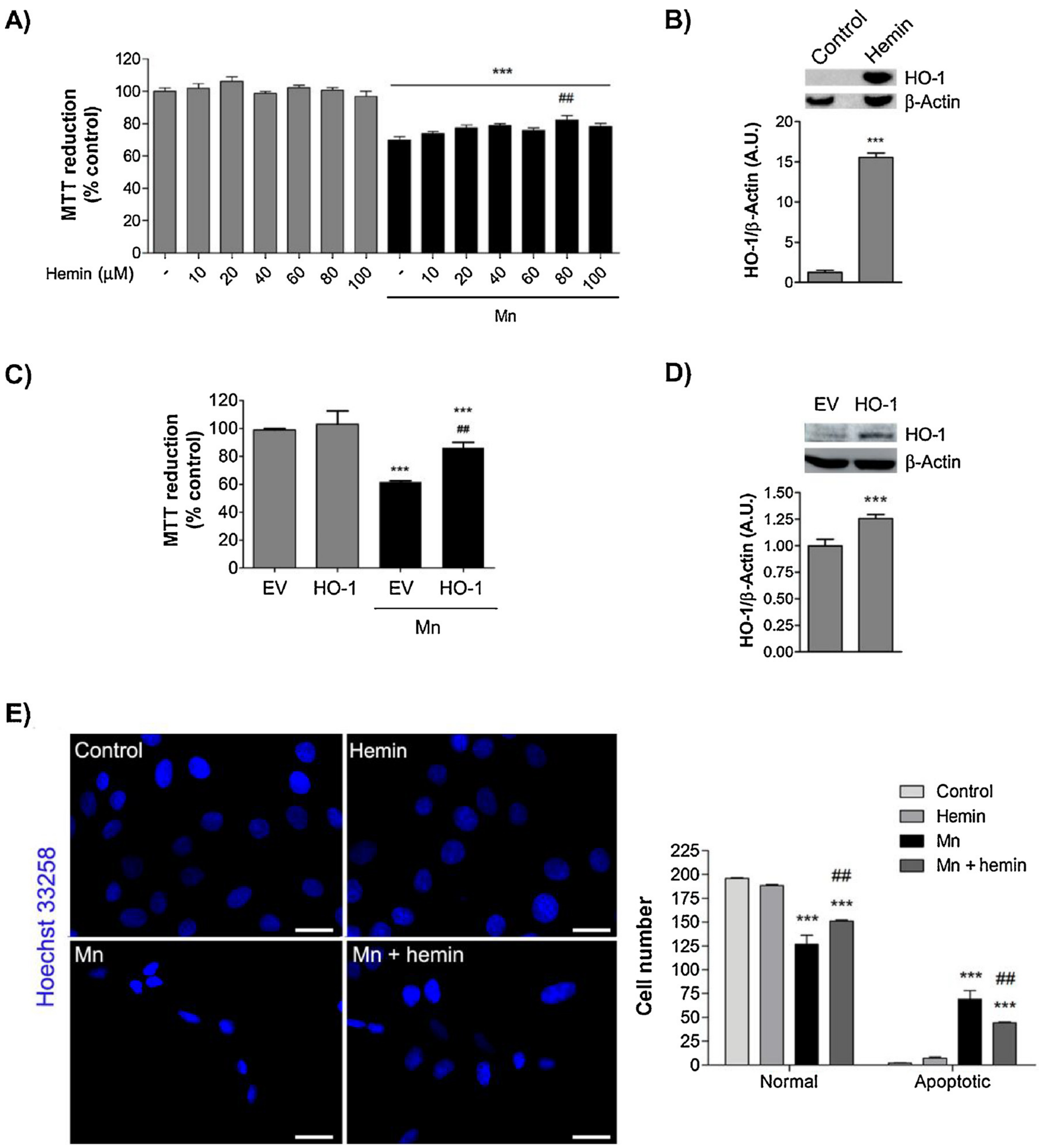

Fig. 3. HO-1 induction is cytoprotective against Mn^{2+}- induced cell death. A. The effect of hemin (10–100 µM) on Mn^{2+}-induced cell death was measured by MTT assay. **B.** Cells were treated with 80 µM hemin for 25 h. HO-1 expression levels were analyzed and normalized to β-Actin. **(C–D)** Cells were transfected with pcDNA3-HO-1 (HO-1) or pcDNA3 empty vector (EV). **C.** Cell viability was measured by MTT after 24 h Mn^{2+} exposure. **D.** HO-1 expression levels were determined by immunoblotting and expressed as a ratio to β-Actin. **E.** Cells were pretreated with 80 µM hemin, exposed to Mn^{2+} for 24 h and stained with Hoechst 33258. Nuclear morphology was visualized by fluorescence microscopy (λ_{em}: 350/50 nm, λ_{ex}: 460/50 nm). The number of cells with apoptotic nuclei was scored (200 cells per sample). Magnification: 100 × . Scale bar: 20 µm. ***$p < 0.001$ vs. control; $^{##}p < 0.01$, $^{###}p < 0.001$ vs. Mn. A.U.: arbitrary units.

activity of several transcription factors involved in mitochondrial biogenesis and function such as the nuclear respiratory factor-1 (NRF-1) (Palikaras et al., 2015).

We evaluated the nuclear levels of PGC-1α (Fig. 8A) and its downstream factor NRF-1 (Fig. 8B) by immunocytochemistry. Whereas Mn^{2+} reduced the nuclear expression of PGC-1α (27 ± 10%, $p < 0.01$) and NRF-1 (25 ± 9%, $p < 0.001$), pre-incubation with hemin was able to restore nuclear expression to control values.

Altogether, these results point to HO-1 as playing a cytoprotective role against Mn^{2+} toxicity by preventing mitochondrial fragmentation and mitophagy and contributing to the biogenesis of new mitochondria through PGC-1α/NRF-1 pathway.

4. Discussion

Brain is particularly susceptible to oxidative damage owing to its large lipids composition, high energy demand, and less abundant antioxidant defenses relative to other organs. Accordingly, ROS damage has been detected within brain regions undergoing neurodegeneration of Parkinson's disease, Alzheimer's disease and amyotrophic lateral sclerosis patients (Andersen, 2004). The persistence of high levels of ROS promotes damage to cell macromolecules leading to the activation of apoptotic and necrotic cell death pathways. Thereby, setting up a proper antioxidant defense is crucial to maintain cellular homeostasis. Particularly, HO-1 is considered an important component of the cellular antioxidant machinery. In the brain, HO pathway has been shown to act

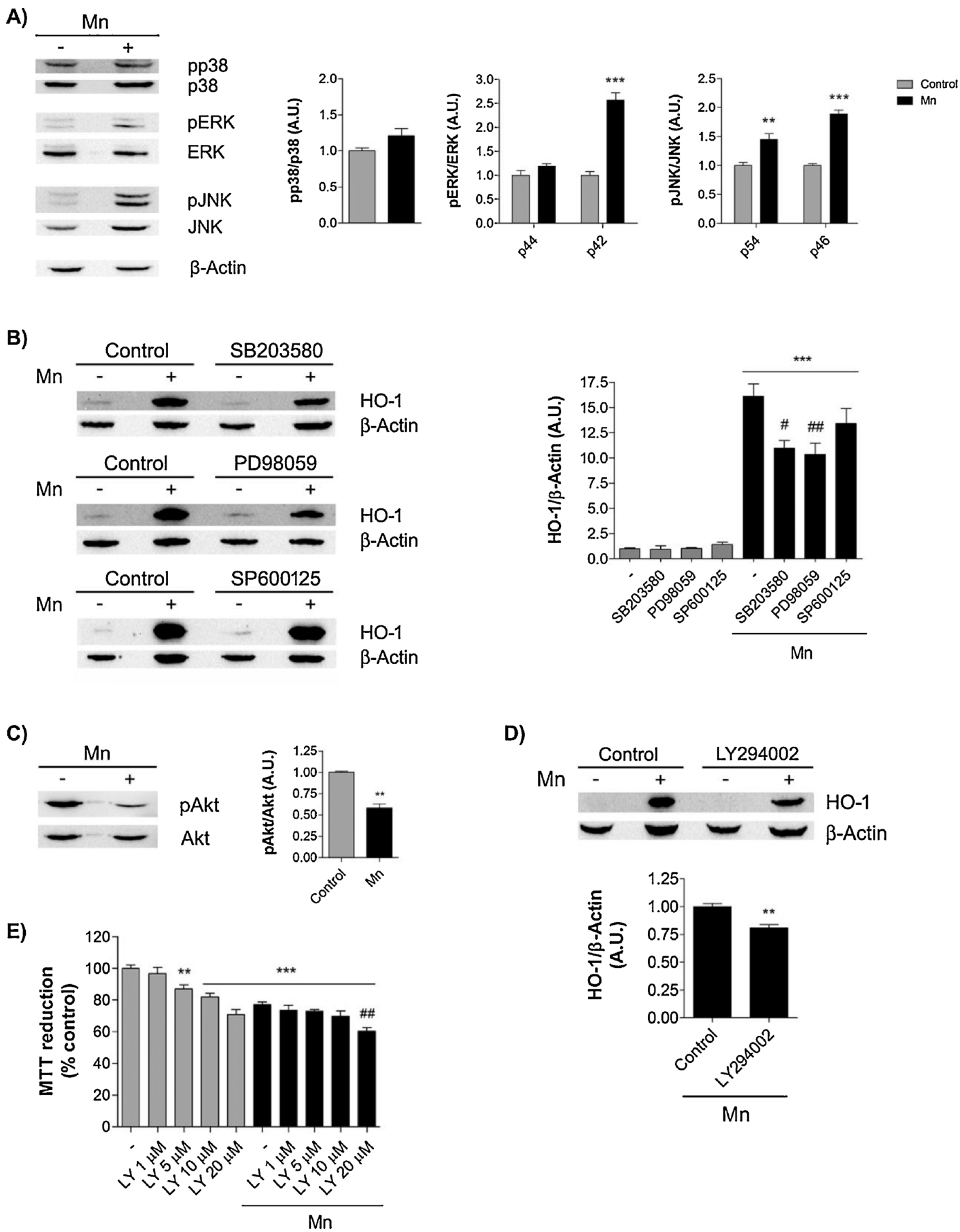

Fig. 4. MAPKs and Akt signaling on Mn^{2+}-induced HO-1 expression. A. Cells were incubated with 750 μM Mn^{2+} for 24 h and lysates were subjected to SDS-PAGE. pp38, pERK and pJNK were revealed by immunoblotting, quantified and normalized to p38, ERK2 and JNK1. **B.** Cells were pre-incubated (1 h) with p38 (SB203580, 10 μM), ERK (PD98059, 25 μM) or JNK (SP600125, 20 μM) inhibitors and HO-1 expression was analyzed by western blotting. Densitometric data was normalized to β-Actin. **C.** Representative western blots of pAkt and total Akt in Mn^{2+}- exposed cells. Images were quantified and normalized to β-Actin. **D.** HO-1 expression levels after 20 μM LY294002 pre-treatment were analyzed by immunoblotting. **E.** Cells were pre-treated (1 h) with 5, 10 or 20 μM LY294002 before Mn^{2+} exposure. Viability was measured by MTT assay. **$p < 0.01$, ***$p < 0.001$ vs. control; $^{\#}p < 0.05$, $^{\#\#}p < 0.01$ vs. Mn. A.U.: arbitrary units.

as a fundamental defensive mechanism for neurons exposed to oxidant challenge (Cuadrado and Rojo, 2008), including Mn-induced oxidative stress (Li et al., 2011a, 2011b; Taka et al., 2012).

The cytoprotective role of HO-1 has been also demonstrated in astrocytes after different insults. However, there is no information about the role of HO-1 in the context of Mn-induced oxidative stress in astrocytes. Thus, we focused on this topic in our experimental *in vitro* model of C6 cells exposed to 750 μM Mn^{2+} where we have already characterized ROS-induced apoptotic cell death (Alaimo et al., 2011; Gorojod et al., 2017). Mn^{2+} up-regulated HO-1 expression (Fig. 1) as

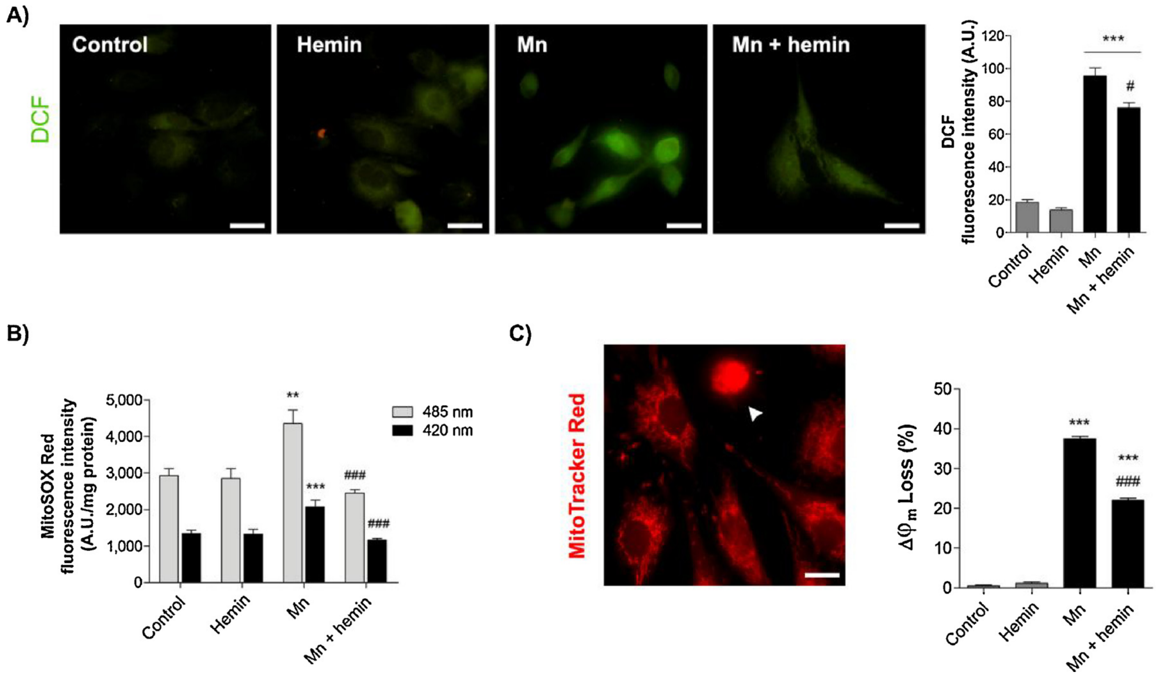

Fig. 5. Hemin prevents ROS generation and Mn^{2+}-induced mitochondrial dysfunction. A. *Total ROS*: cells were loaded with DCDHF-DA (10 μM) (λ_{em}: 450–490 nm, λ_{ex}: 515 nm) and representative images of DCF fluorescence were obtained. Magnification: 100 × . Scale bar: 20 μm. Green DCF fluorescence intensity was quantified using ImageJ software. **B.** *Mitochondrial ROS:* cells were loaded with MitoSOX Red (5 μM) and fluorescence intensity was measured by spectrofluorometry (λ_{ex}: 420 or 485 nm, λ_{em}: 590 nm). **C.** Cells were stained with MitoTracker Red CMXRos (75 nM) and analyzed by fluorescence microscopy. Cells with loss of mitochondrial transmembrane potential (Δφm, white arrowheads) were identified and scored. Magnification: 100 × . Scale bar: 10 μm. $^{**}p < 0.01$, $^{***}p < 0.001$ vs. control; $^{\#}p < 0.05$, $^{\#\#\#}p < 0.001$ vs. Mn. A.U.: arbitrary units(For interpretation of the references to colour in this figure legend, the reader is referred to the web version of this article.).

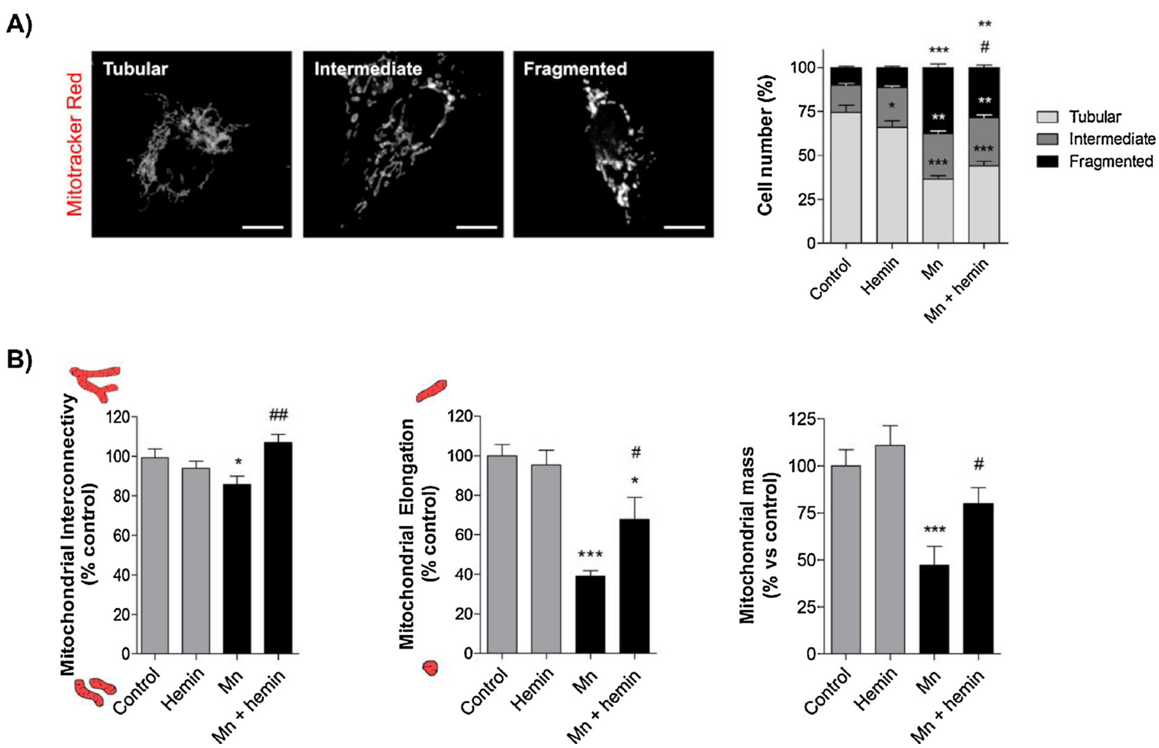

Fig. 6. Hemin contributes to maintain the mitochondrial network integrity. A. Mitochondria were labelled with 75 nM MitoTracker Red CMXRos and visualized by fluorescence microscopy (λ_{ex}: 543/20 nm; λ_{em}: 593/40 nm). Magnification: 60 × . 200 cells/ sample were scored and classified in three categories accordingly to the mitochondrial morphology exhibited: tubular (normal), intermediate (mixed) and fragmented (small, rounded and/or swollen). **B.** Quantification of mitochondrial interconnectivity, elongation and mass (Mito-Morphology macro, ImageJ). $^{*}p < 0.05$, $^{**}p < 0.01$, $^{***}p < 0.001$ vs. control; $^{\#}p < 0.05$, $^{\#\#}p < 0.01$ vs. Mn(For interpretation of the references to colour in this figure legend, the reader is referred to the web version of this article.).

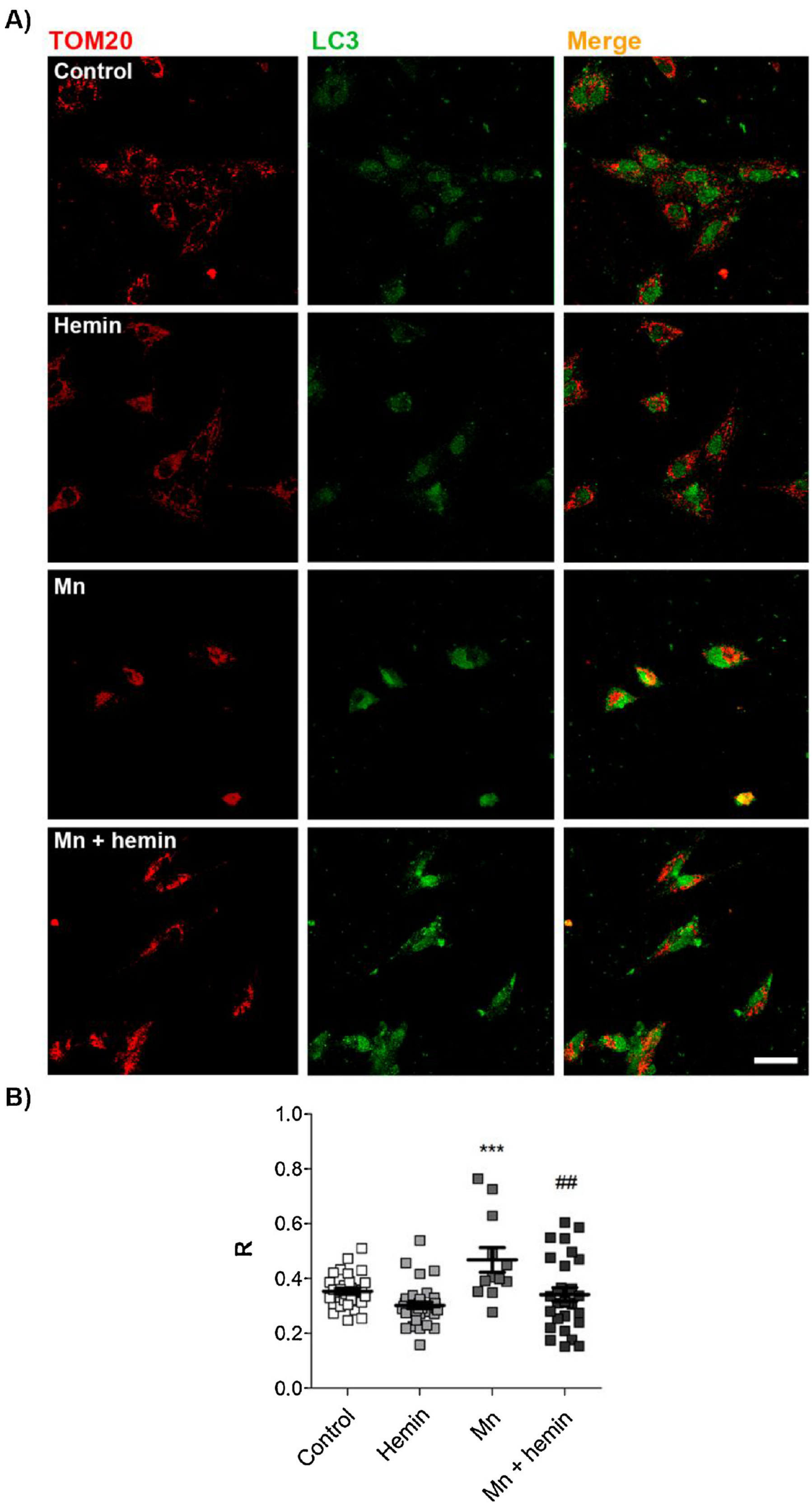

Fig. 7. Effect of hemin on Mn^{2+}-induced mitophagy. Immunocytochemical detection of TOM-20 (red) and LC3 (green) was performed to label mitochondria and autophagosomes, respectively (Alexa 555, λ_{ex}: 543 nm, λ_{em}: 585–605 nm; Alexa 488, λ_{ex}: 488 nm, λ_{em}: 515–530 nm). **A.** Representative confocal microscopy images of each condition. Scale bar: 10 µm. **B.** Manders' overlap coefficient (R) was employed to quantify the degree of co-localization between TOM-20 and LC3. ***p < 0.001 vs. control and ##p < 0.01 vs. Mn(For interpretation of the references to colour in this figure legend, the reader is referred to the web version of this article.).

reported in neuron-like PC12 (Li et al., 2011a, 2011b; Taka et al., 2012; Jin et al., 2017) and microglial BV-2 cells (Park and Chun, 2017). To elucidate the role of this protein in Mn^{2+} toxicity, we next performed experiments by modulating its activity. The inhibition of HO-1 by SnPP (Kappas and Drummond, 1986) potentiated both Mn^{2+}-induced appearance of apoptotic nuclei and increased cell death (Figs. 2**A and C**). Similar results were obtained by Srisook et al. (2005) who found that HO-1 inhibition sensitized C6 cells to Cd-induced toxicity. SnPP also

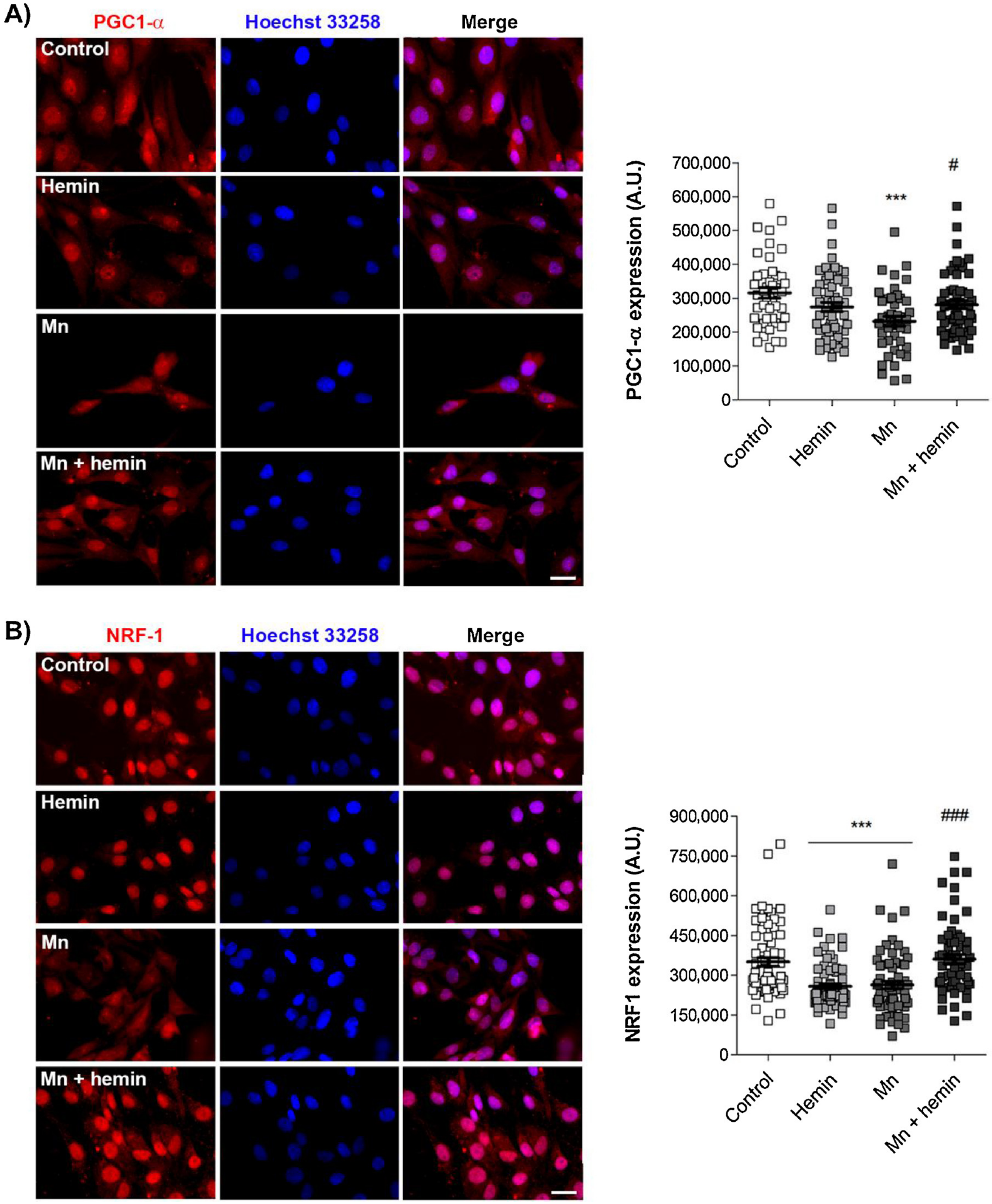

Fig. 8. Hemin maintains the nuclear PGC-1α and NRF-1 levels in Mn^{2+}- exposed cells. Cells were immunolabeled with anti- **(A)** PGC-1α or **(B)** NRF-1 antibodies (red) and nuclei were counterstained with Hoechst 33,258 (blue). Representative fluorescence images of each treatment are shown. Magnification: 100 ×. Scale bar: 20 μm. **(A)** PGC-1α and **(B)** NRF-1 expression levels in the nuclear compartment were quantified using ImageJ software. $^{***}p < 0.001$ vs. control and $^{\#}p < 0.05$, $^{\#\#\#}p < 0.001$ vs. Mn. A.U.: arbitrary units(For interpretation of the references to colour in this figure legend, the reader is referred to the web version of this article.).

induced an increase in HO-1 expression levels (Fig. 2B), an effect previously attributed to a positive feedback loop caused by HO-1 inhibition (Sardana and Kappas, 1987). To add evidence about HO-1-mediated cytoprotection, its expression was up-regulated by both a pharmacological and genetic strategies. Hemin, a known selective HO-1 inducer, has previously proved to increase HO-1 activity (10 μM) and mRNA levels (50–100 μM) in C6 cells (Schmidt et al., 1999). In our model, pre-incubation with 80 μM hemin enhanced Mn^{2+}-induced HO-1 up-regulation and prevented the appearance of apoptotic nuclei as well as cell death (Figs. 3**A, B and E**). Accordingly, genetic HO-1 overexpression was able to preserve cell viability (Figs. 3**C and D**). These results support a role for HO-1 in protecting cellular integrity towards Mn insult.

Several studies have shown that MAPKs (ERK, JNK and p38) as well as PI3K/Akt regulate HO-1 expression in response to diverse stimuli. Interestingly, Mn^{2+} activates these MAPKs in a time- and dose-dependent manner in cultured rat astrocytes (Exil et al., 2014) and C6 cells (Gorojod et al., 2015). In particular, our previous work showed that 750 μM Mn^{2+} exposure for 6 h in C6 cells increases both p-ERK and p-JNK and decreases p-Akt levels (Gorojod et al., 2015). In the present report, we demonstrate that ERK, p38 and Akt are involved in HO-1 up-regulation after 24 h Mn^{2+} exposure (Fig. 4**B and D**). Considering that Mn-mediated HO-1 induction in PC12 cells is not regulated by MAPKs (Li et al., 2011a), our results suggest that different mechanisms could operate in neurons and glial cells to induce HO-1 after Mn exposure.

Mitochondria are the major source and target of intracellular ROS. Under physiological conditions, ROS act as redox signaling messengers. However, when antioxidants/ROS balance is disrupted, elevated ROS levels produce oxidative damage of mitochondrial DNA and proteins, leading to electron transport chain disruption, decrease in ATP production and $\Delta\varphi$m dissipation (Fernández-Checa et al., 2010). Mn overexposure has been widely associated to oxidative stress and mitochondrial damage (Gonzalez et al., 2008; Prabhakaran et al., 2009; Alaimo et al., 2011; Jiang et al., 2014). In the present study, we demonstrated that hemin prevented the increase of total (Fig. 5A) and mitochondrial (Fig. 5B) ROS levels and contributed to the $\Delta\varphi$m preservation (Fig. 5C). Based on the aforementioned findings, we hypothesized that HO-1 is induced, at least in part, to preserve a pool of healthy mitochondria.

The landscape of mitochondrial research in the biomedical field has become a hot spot in the last few years. Particularly, the MQC regulation represents a potentially useful, but relatively unexplored area for therapeutic innovation (Suliman and Piantadosi, 2016). Hitherto, limited effort has been made to understand the interplay between HO-1 and the MQC. In the current study, we revealed that HO-1 preserves all MQC programs in astroglial cells undergoing Mn^{2+}-induced oxidative injury. First, we focused on mitochondrial dynamics. Evidence obtained demonstrates that HO-1 exerts a protective role on Mn^{2+}-injured cells, by preserving the mitochondrial fusion/fission balance (Fig. 6). To our knowledge, there is only one report about the role of HO-1 in modulating the MQC in an oxidative injury model in the heart (Hull et al., 2016). There, HO-1 overexpression in mice inhibited the upregulation of the mitochondrial fission mediator Fis1 and increased the expression of the fusion mediators, Mfn1 and Mfn2. Shortly after, Yu et al. (2016a, 2016b), employing models of LPS-induced acute lung injury/acute respiratory distress syndrome and LPS-treated alveolar macrophages, demonstrated that hemin pre-treatment prevented the LPS-induced changes in the fusion and fission proteins levels. Thus, these authors added data in favor of HO-1 attenuating oxidative injury through the modulation of mitochondrial dynamics.

Secondly, we focused on mitophagy, a crucial MQC program, in charge of degrading damaged or redundant mitochondria excluded from the mitochondrial network by the fission process (Kroemer et al., 2010). In previous work, we have already described autophagy as a protective mechanism against Mn^{2+} injury in C6 cells (Gorojod et al., 2015). Here, we proved that hemin decreases the mitochondrial clearance induced by Mn^{2+} (Fig. 7). These findings support our aforementioned hypothesis that HO-1 contributes to preserve a healthy mitochondrial population. Similarly, Hull et al. (2016) showed that the protective effects of HO-1 overexpression where mediated by the maintenance of the mitophagic pathway at homeostatic levels.

Mitophagy acts coordinately with mitochondrial biogenesis to maintain proper energy levels in response to cellular metabolic state, stress and other intracellular or environmental signals. Particularly, mitochondrial biogenesis is defined as the set of molecular instructions by which cells replace or increase their mitochondria through the proliferation of pre-existing organelles (Palikaras et al., 2015; Suliman and Piantadosi, 2016). An imbalance between mitochondrial degradation and proliferation events contributes to various pathological conditions, including neurodegenerative diseases (Palikaras et al., 2015).

As we mentioned above, biogenesis is regulated by nuclear transcription factors, such as NRF-1 and its coactivator PGC-1α (Palikaras et al., 2015). We demonstrated that Mn^{2+} treatment decreases the nuclear levels of PGC-1α and its downstream factor NRF-1 along with a mitochondrial mass reduction (Figs. 6B and 8). In contrast, Exil et al. (2014) reported that rat primary astrocytes exposed to Mn (100 and 500 μM; 6 and 24 h) exhibited elevated PGC-1α levels. This apparent controversy could be due to the fact that we employed nuclear fractions for western blot analysis while Exil et al. (2014) used total lysates. In accordance with our findings, Zheng et al. (2010) demonstrated that the bioenergetics-related genes responsive to the master regulator PGC-1α are under-expressed in the *substantia nigra* of Parkinson's disease (PD) patients. Taken together, evidence accumulated point out to PGC-1α and NRF-1 as potential molecular targets associated with defective mitochondrial function caused by different cytotoxic insults.

Incubation with hemin prior to Mn^{2+} addition increased the mitochondrial mass and restored the PGC-1α and NRF-1 nuclear expression levels compared with Mn^{2+}-treatment (Figs. 6B and 8). These results support a role for HO-1 in promoting mitochondrial biogenesis. This role may be mediated by two mechanisms: i) HO-1 generates a feed-forward loop to induce the NRF-1 transcription, ii), HO-1 phosphorylates Akt which in turn phosphorylates NRF-1 leading to its nuclear translocation (Piantadosi et al., 2008, 2011; MacGarvey et al., 2012). Previous data obtained by Hull et al. (2016) demonstrated that HO-1 overexpression in mice promotes mitochondrial biogenesis by up-regulating PGC-1α, NRF-1 and TFAM expression. These findings demonstrated a role for HO-1 in regulating the mitochondrial biogenesis.

5. Conclusion

Our results demonstrate that Mn^{2+} markedly induces HO-1 expression in astroglial C6. This increase in HO-1 expression is relevant for preventing both ROS generation and Mn^{2+}-induced apoptosis. Remarkably, we provide the first evidence demonstrating that HO-1 expression after Mn^{2+} overexposure appears to have a generally protective effect on MQC by influencing the processes of mitochondrial dynamics, mitophagy and biogenesis. Altogether, our findings support the proposal that HO-1 could be considered as a promising therapeutic target for Manganism and probably other related neurological diseases where oxidative stress and mitochondrial dysfunction play a critical role.

Conflict of interest

The authors declare no conflict of interest.

The Transparency document associated with this article can be found in the online version.

Aknowledgements

This work was supported by grants from the Consejo Nacional de Investigaciones Científicas y Técnicas (CONICET PIP 5406 and 0771). R.M.G., S.P.A., J.H.M. were supported by CONICET scholarships. M.E.C was supported by a Bunge and Born scholarship. A.A., E.S.V. and M.L.K. are researcher members at CONICET.

References

Agarwal, A., Bolisetty, S., 2013. Adaptive responses to tissue injury: role of heme Oxygenase-1. Trans. Am. Clin. Climatol. Assoc. 124, 111–122.
Alaimo, A., Gorojod, R.M., Kotler, M.L., 2011. The extrinsic and intrinsic apoptotic pathways are involved in manganese toxicity in rat astrocytoma C6 cells. Neurochem. Int. 59, 297–308. https://doi.org/10.1016/j.neuint.2011.06.001.
Alaimo, A., Gorojod, R.M., Miglietta, E.A., Villarreal, A., Ramos, A.J., Kotler, M.L., 2013. Manganese induces mitochondrial dynamics impairment and apoptotic cell death: a study in human Gli36 cells. Neurosci. Lett. 554, 76–81. https://doi.org/10.1016/j.neulet.2013.08.061.
Alaimo, A., Gorojod, R.M., Beauquis, J., Muñoz, M.J., Saravia, F., Kotler, M.L., 2014. Deregulation of mitochondria-shaping proteins Opa-1 and Drp-1 in manganese-induced apoptosis. PLoS ONE 9, e91848. https://doi.org/10.1371/journal.pone.0091848.
Andersen, J.K., 2004. Oxidative stress in neurodegeneration: cause or consequence? Nat. Med. 10, S18–25. https://doi.org/10.1038/nrn1434.
Aschner, M., Gannon, M., Kimelberg, H.K., 1992. Manganese uptake and efflux in

cultured rat astrocytes. J. Neurochem. 58, 730–735.
Cuadrado, A., Rojo, A.I., 2008. Heme oxygenase-1 as a therapeutic target in neurodegenerative diseases and brain infections. Curr. Pharm. Des. 14, 429–442.
Dagda, R.K., Cherra, S.J., Kulich, S.M., Tandon, A., Park, D., Chu, C.T., 2009. Loss of PINK1 function promotes mitophagy through effects on oxidative stress and mitochondrial fission. J. Biol. Chem. 284, 13843–13855. https://doi.org/10.1074/jbc.M808515200.
Dupuis, L., 2014. Mitochondrial quality control in neurodegenerative diseases. Biochimie 100, 177–183. https://doi.org/10.1016/j.biochi.2013.07.033.
Exil, V., Ping, L., Yu, Y., Chakraborty, S., Caito, S.W., Wells, K.S., Karki, P., Lee, E., Aschner, M., 2014. Activation of MAPK and FoxO by manganese (Mn) in rat neonatal primary astrocyte cultures. PLoS ONE 9, e94753. https://doi.org/10.1371/journal.pone.0094753.
Fernández-Checa, J.C., Fernández, A., Morales, A., Marí, M., García-Ruiz, C., Colell, A., 2010. Oxidative stress and altered mitochondrial function in neurodegenerative diseases: lessons from mouse models. CNS Neurol. Disord. Drug Targets 9, 439–454.
Gonzalez, L.E., Juknat, A.A., Venosa, A.J., Verrengia, N., Kotler, M.L., 2008. Manganese activates the mitochondrial apoptotic pathway in rat astrocytes by modulating the expression of proteins of the Bcl-2 family. Neurochem. Int. 53, 408–415. https://doi.org/10.1016/j.neuint.2008.09.008.
Gorojod, R.M., Alaimo, A., Porte Alcon, S., Pomilio, C., Saravia, F., Kotler, M.L., 2015. The autophagic- lysosomal pathway determines the fate of glial cells under manganese- induced oxidative stress conditions. Free Radic. Biol. Med. 87, 237–251. https://doi.org/10.1016/j.freeradbiomed.2015.06.034.
Gorojod, R.M., Alaimo, A., Porte Alcon, S., Saravia, F., Kotler, M.L., 2017. Interplay between lysosomal, mitochondrial and death receptor pathways during manganese-induced apoptosis in glial cells. Arch. Toxicol. 91, 3065–3078. https://doi.org/10.1007/s00204-017-1936-7.
Gozzelino, R., Jeney, V., Soares, M.P., 2010. Mechanisms of cell protection by heme oxygenase-1. Annu. Rev. Pharmacol. Toxicol. 50, 323–354. https://doi.org/10.1146/annurev.pharmtox.010909.105600.
Gunter, T.E., Gavin, C.E., Aschner, M., Gunter, K.K., 2006. Speciation of manganese in cells and mitochondria: a search for the proximal cause of manganese neurotoxicity. Neurotoxicology 27, 765–776. https://doi.org/10.1016/j.neuro.2006.05.002.
Hettiarachchi, N.T., Boyle, J.P., Dallas, M.L., Al-Owais, M.M., Scragg, J.L., Peers, C., 2017. Heme oxygenase-1 derived carbon monoxide suppresses $A\beta_{1-42}$ toxicity in astrocytes. Cell Death Dis. 8, e2884. https://doi.org/10.1038/cddis.2017.276.
Hull, T.D., Boddu, R., Guo, L., Tisher, C.C., Traylor, A.M., Patel, B., Joseph, R., Prabhu, S.D., Suliman, H.B., Piantadosi, C.A., Agarwal, A., George, J.F., 2016. Heme oxygenase-1 regulates mitochondrial quality control in the heart. JCI Insight 1, e85817. https://doi.org/10.1172/jci.insight.85817.
Jiang, J.K., Ma, X., Wu, Q.Y., Qian, W.B., Wang, N., Shi, S.S., Han, J.L., Zhao, J.Y., Jiang, S.Y., Wan, C.H., 2014. Upregulation of mitochondrial protease HtrA2/Omi contributes to manganese-induced neuronal apoptosis in rat brain striatum. Neuroscience 268, 169–179. https://doi.org/10.1016/j.neuroscience.2014.03.003.
Jin, Y., Liu, X., Liu, H., Chen, S., Gao, C., Ge, K., Zhang, C., Zhang, J., 2017. Oxidative stress-induced apoptosis of osteoblastic MC3T3-E1 cells by hydroxyapatite nanoparticles through lysosomal and mitochondrial pathways. RSC Adv. 7, 13010–13018. https://doi.org/10.1039/C7RA01008G.
Kappas, A., Drummond, G.S., 1986. Control of heme metabolism with synthetic metalloporphyrins. J. Clin. Invest. 77, 335–339. https://doi.org/10.1172/JCI112309.
Kappas, A., Drummond, G.S., Simionatto, C.S., Anderson, K.E., 1984. Control of heme oxygenase and plasma levels of bilirubin by a synthetic heme analogue, tin-protoporphyrin. Hepatology 4, 336–341.
Kroemer, G., Mariño, G., Levine, B., 2010. Autophagy and the integrated stress response. Mol. Cell 40, 280–293. https://doi.org/10.1016/j.molcel.2010.09.023.
Li, H., Wu, S., Shi, N., Lian, S., Lin, W., 2011a. Nrf2/HO-1 pathway activation by manganese is associated with reactive oxygen species and ubiquitin-proteasome pathway, not MAPKs signaling. J. Appl. Toxicol. 31, 690–697. https://doi.org/10.1002/jat.1654.
Li, H., Wu, S., Shi, N., Lin, W., You, J., Zhou, W., 2011b. NF-E2-related factor 2 activation in PC12 cells: its protective role in manganese-induced damage. Arch. Toxicol. 85, 901–910. https://doi.org/10.1007/s00204-010-0625-6.
MacGarvey, N.C., Suliman, H.B., Bartz, R.R., Fu, P., Withers, C.M., Welty-Wolf, K.E., Piantadosi, C.A., 2012. Activation of mitochondrial biogenesis by heme oxygenase-1-mediated NF-E2-related factor-2 induction rescues mice from lethal Staphylococcus aureus sepsis. Am. J. Respir. Crit. Care Med. 185, 851–861. https://doi.org/10.1164/rccm.201106-1152OC.
Martin, D., Rojo, A.I., Salinas, M., Diaz, R., Gallardo, G., Alam, J., De Galarreta, C.M.R., Cuadrado, A., 2004. Regulation of heme oxygenase-1 expression through the phosphatidylinositol 3-kinase/Akt pathway and the Nrf2 transcription factor in response to the antioxidant phytochemical carnosol. J. Biol. Chem. 279, 8919–8929. https://doi.org/10.1074/jbc.M309660200.
Milatovic, D., Yin, Z., Gupta, R.C., Sidoryk, M., Albrecht, J., Aschner, J.L., Aschner, M., 2007. Manganese induces oxidative impairment in cultured rat astrocytes. Toxicol. Sci. 98, 198–205. https://doi.org/10.1093/toxsci/kfm095.
Morita, K., Lee, M.-S., Her, S., 2009. Possible relation of hemin-induced HO-1 expression to the upregulation of VEGF and BDNF mRNA levels in rat C6 glioma cells. J. Mol. Neurosci. 38, 31–40. https://doi.org/10.1007/s12031-008-9156-5.
Palikaras, K., Lionaki, E., Tavernarakis, N., 2015. Balancing mitochondrial biogenesis and mitophagy to maintain energy metabolism homeostasis. Cell Death Differ. 22, 1399–1401. https://doi.org/10.1038/cdd.2015.86.
Park, E., Chun, H.S., 2017. Protective effects of curcumin on manganese-induced BV-2 microglial cell death. Biol. Pharm. Bull. 40, 1275–1281. https://doi.org/10.1248/bpb.b17-00160.
Piantadosi, C.A., Carraway, M.S., Babiker, A., Suliman, H.B., 2008. Heme oxygenase-1 regulates cardiac mitochondrial biogenesis via Nrf2-mediated transcriptional control of nuclear respiratory factor-1. Circ. Res. 103, 1232–1240. https://doi.org/10.1161/01.RES.0000338597.71702.ad.
Piantadosi, C.A., Withers, C.M., Bartz, R.R., MacGarvey, N.C., Fu, P., Sweeney, T.E., Welty-Wolf, K.E., Suliman, H.B., 2011. Heme oxygenase-1 couples activation of mitochondrial biogenesis to anti-inflammatory cytokine expression. J. Biol. Chem. 286, 16374–16385. https://doi.org/10.1074/jbc.M110.207738.
Prabhakaran, K., Chapman, G.D., Gunasekar, P.G., 2009. BNIP3 up-regulation and mitochondrial dysfunction in manganese-induced neurotoxicity. Neurotoxicology 30, 414–422. https://doi.org/10.1016/j.neuro.2009.02.012.
Robinson, K.M., Janes, M.S., Beckman, J.S., 2008. The selective detection of mitochondrial superoxide by live cell imaging. Nat. Protoc. 3, 941–947. https://doi.org/10.1038/nprot.2008.56.
Roth, J.A., 2009. Are there common biochemical and molecular mechanisms controlling manganism and parkisonism. Neuromolecular Med. 11, 281–296. https://doi.org/10.1007/s12017-009-8088-8.
Ryter, S.W., Choi, A.M.K., 2002. Heme oxygenase-1: molecular mechanisms of gene expression in oxygen-related stress. Antioxid. Redox Signal. 4, 625–632. https://doi.org/10.1089/15230860260220120.
Ryter, S.W., Xi, S., Hartsfield, C.L., Choi, A.M.K., 2002. Mitogen activated protein kinase (MAPK) pathway regulates heme oxygenase-1 gene expression by hypoxia in vascular cells. Antioxid. Redox Signal. 4, 587–592. https://doi.org/10.1089/15230860260220085.
Ryter, S.W., Alam, J., Choi, A.M.K., 2006. Heme Oxygenase-1/Carbon monoxide: from basic science to therapeutic applications. Physiol. Rev. 86, 583–650. https://doi.org/10.1152/physrev.00011.2005.
Sardana, M.K., Kappas, A., 1987. Dual control mechanism for heme oxygenase: tin(IV)-protoporphyrin potently inhibits enzyme activity while markedly increasing content of enzyme protein in liver. Proc. Natl. Acad. Sci. U.S.A. 84, 2464–2468.
Schipper, H.M., 2011. Heme oxygenase-1 in Alzheimer disease: a tribute to Moussa Youdim. J. Neural Transm. 118, 381–387. https://doi.org/10.1007/s00702-010-0436-1.
Schmidt, J., Mertz, K., Morgan, J.I., 1999. Regulation of heme oxygenase-1 expression by dopamine in cultured C6 glioma and primary astrocytes. Brain Res. Mol. Brain Res. 73, 50–59.
Sridharan, S., Jain, K., Basu, A., 2011. Regulation of autophagy by kinases. Cancers 3, 2630–2654. https://doi.org/10.3390/cancers3022630.
Srisook, K., Jung, N.-H., Kim, B.-R., Cha, S.-H., Kim, H.-S., Cha, Y.-N., 2005. Heme oxygenase-1-mediated partial cytoprotective effect by NO on cadmium-induced cytotoxicity in C6 rat glioma cells. Toxicol. In Vitro 19, 31–39. https://doi.org/10.1016/j.tiv.2004.04.012.
Suliman, H.B., Piantadosi, C.A., 2016. Mitochondrial quality control as a therapeutic target. Pharmacol. Rev. 68, 20–48. https://doi.org/10.1124/pr.115.011502.
Taka, E., Mazzio, E., Soliman, K.F.A., Renee Reams, R., 2012. Microarray genomic profile of mitochondrial and oxidant response in manganese chloride treated PC12 cells. Neurotoxicology 33, 162–168. https://doi.org/10.1016/j.neuro.2012.01.001.
Tenhunen, R., Marver, H.S., Schmid, R., 1968. The enzymatic conversion of heme to bilirubin by microsomal heme oxygenase. Proc. Natl. Acad. Sci. U.S.A. 61, 748–755.
Tenhunen, R., Marver, H.S., Schmid, R., 1970. The enzymatic catabolism of hemoglobin: stimulation of microsomal heme oxygenase by hemin. J. Lab. Clin. Med. 75, 410–421.
Wada, T., Penninger, J.M., 2004. Mitogen-activated protein kinases in apoptosis regulation. Oncogene 23, 2838–2849. https://doi.org/10.1038/sj.onc.1207556.
Wagener, F.A.D.T.G., Volk, H.-D., Willis, D., Abraham, N.G., Soares, M.P., Adema, G.J., Figdor, C.G., 2003. Different faces of the heme-Heme oxygenase system in inflammation. Pharmacol. Rev. 55, 551–571. https://doi.org/10.1124/pr.55.3.5.
Westermann, B., 2010. Mitochondrial fusion and fission in cell life and death. Nat. Rev. Mol. Cell Biol. 11, 872–884. https://doi.org/10.1038/nrm3013.
Yu, J., Shi, J., Wang, D., Dong, S., Zhang, Y., Wang, M., Gong, L., Fu, Q., Liu, D., 2016a. Heme Oxygenase-1/Carbon monoxide-regulated mitochondrial dynamic equilibrium contributes to the attenuation of endotoxin-induced acute lung injury in rats and in lipopolysaccharide-activated macrophages. Anesthesiology 125, 1190–1201. https://doi.org/10.1097/ALN.0000000000001333.
Yu, J., Wang, Y., Li, Z., Dong, S., Wang, D., Gong, L., Shi, J., Zhang, Y., Liu, D., Mu, R., 2016b. Effect of heme Oxygenase-1 on Mitofusin-1 protein in LPS-induced ALI/ARDS in rats. Sci. Rep. 6, 36530. https://doi.org/10.1038/srep36530.
Zhang, X., Bedard, E.L., Potter, R., Zhong, R., Alam, J., Choi, A.M.K., Lee, P.J., 2002. Mitogen-activated protein kinases regulate HO-1 gene transcription after ischemia-reperfusion lung injury. Am. J. Physiol. Lung Cell Mol. Physiol. 283, L815–829. https://doi.org/10.1152/ajplung.00485.2001.
Zheng, B., Liao, Z., Locascio, J.J., Lesniak, K.A., Roderick, S.S., Watt, M.L., Eklund, A.C., Zhang-James, Y., Kim, P.D., Hauser, M.A., Grünblatt, E., Moran, L.B., Mandel, S.A., Riederer, P., Miller, R.M., Federoff, H.J., Wüllner, U., Papapetropoulos, S., Youdim, M.B., Cantuti-Castelvetri, I., Young, A.B., Vance, J.M., Davis, R.L., Hedreen, J.C., Adler, C.H., Beach, T.G., Graeber, M.B., Middleton, F.A., Rochet, J.C., Scherzer, C.R., Global PD Gene Expression (GPEX) Consortium, 2010. PGC-1α, a potential therapeutic target for early intervention in Parkinson's disease. Sci. Transl. Med. 2, 52ra73. https://doi.org/10.1126/scitranslmed.3001059.